Fluctuations in the number of irreversibly adsorbed particles

Zbigniew Adamczyk,[a] Lilianna Szyk-Warszyńska, B. Siwek, and P. Weroński
Institute of Catalysis and Surface Chemistry Polish Academy of Science, Niezapominajek 8, 30-239 Cracow, Poland

(Received 17 May 2000; accepted 25 September 2000)

Fluctuations in the number of colloid particles adsorbed irreversibly under pure diffusion transport conditions were determined as a function of surface density and ionic strength of the suspension. The experiments were carried out for monodisperse polystyrene latex particles of micrometer size range adsorbing irreversibly at mica surface. The surface density of adsorbed particles at various areas was determined using the direct microscope observation method. A new experimental cell was used enabling *in situ* observations of particles adsorption under conditions of negligible gravity effects. It was found that the particle density fluctuations for high ionic strength were in a good agreement with the theoretical results derived from the random sequential adsorption (RSA) model. Also, the theoretical results stemming from the equilibrium scaled particle theory reflected the experimental data satisfactorily. For lower ionic strength a deviation from the hard sphere behavior was experimentally demonstrated. This effect due to the repulsive electrostatic interactions was interpreted in terms of the effective hard particle concept. The universal dependence of variance on particle density obtained in this way was found in a good agreement with the RSA model for all ionic strength. These results proved that fluctuations in particle density of monolayer formed under diffusional conditions differ fundamentally from these obtained under ballistic transport conditions.
 [S0021-9606(00)71547-9]

I. INTRODUCTION

Knowledge of colloid and bioparticle adsorption mechanisms at solid/liquid interfaces is relevant for polymer and colloid science, biophysics, and medicine, enabling one to control protein and cell separation, enzyme immobilization, thrombosis, biofouling of membranes and artificial organs, etc. Furthermore, by measuring particle adsorption in model systems accessible for direct microscope studies, e.g., monodisperse colloid suspension, important information can be gained concerning mechanisms and kinetics of molecular adsorption difficult to study in a direct way. One of the attractive possibilities is the modeling by colloid systems density fluctuations occurring in adsorbed molecular layers, e.g., proteins or surfactants. It should be remembered that molecular adsorption (including the important case of macromolecule and protein adsorption) is proceeding under diffusion controlled transport with negligible role of convection or external force. Therefore, in order to match closely the molecular adsorption pathways, the model colloid adsorption studies should preferably be carried out for monolayers obtained under diffusion transport conditions. This would also minimize the irreversibility effects pertinent to colloid particle adsorption at solid interfaces.

Despite the significance of this problem, few experimental works were reported in the literature dealing with density fluctuations in adsorbed colloid monolayers. The exceptions are the measurements reported in Refs. 1–4, dealing with the case of external force (gravity) driven colloid particle adsorption, referred to as the ballistic adsorption mechanism. The particle density fluctuations were quantitatively expressed in terms of the reduced variance $\overline{\sigma}^2=\sigma^2/\langle N_p\rangle$ (where σ is the standard deviation of the number of adsorbed particles and $\langle N_p\rangle$ is the averaged number of particles per given surface area). A very interesting finding of these works was that, despite a considerable difference in the pair correlation functions, in all cases the functional dependence of $\overline{\sigma}^2$ on particle density was of similar character, close to the ballistic model predictions.[1–4] This contradiction was interpreted in Ref. 4 as due to finite probability of particle readsorption after an initial unsuccessful adsorption attempt.

Other results reported in the literature[5,6] for the case of a weak external force were in agreement with the RSA model, rather than with the ballistic model. Quite unexpectidly, the results pertinent to equilibrium systems also reflected the experimental data well. However, these results were obtained under conditions when the gravity and hydrodynamic effects due to fluid convection could influence particle adsorption mechanism. Therefore, the motivations of the present study were to determine particle density fluctuations under purely diffusion-controlled transport conditions with the external force and convection effects entirely eliminated. This was achieved by using a new experimental cell with the microscope oriented horizontally, so gravity was directed parallel to the adsorption plane. A further advantage in comparison with previously used arrangements[7–9] is the option of *in situ* observation of adsorbed particle monolayer without drying up the sample.

[a]Author to whom correspondence should be addressed. Electronic mail: ncadamcz@cyf-kr.edu.pl

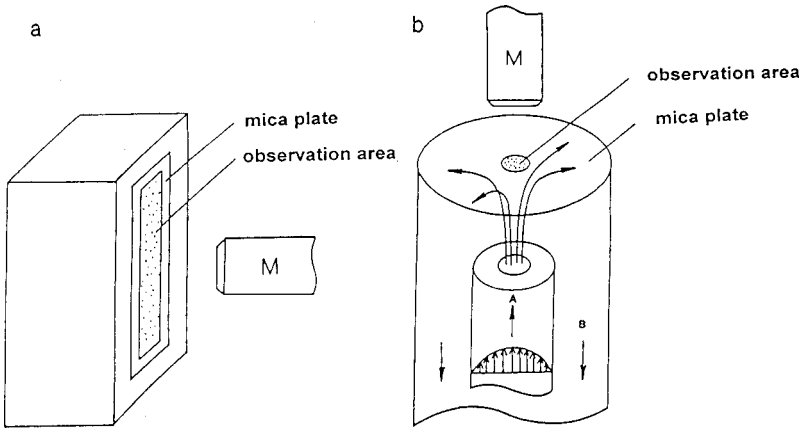

FIG. 1. A schematic view of the experimental cells: (a) the diffusion cell (DC); (b) the radial impinging-jet cell.

II. EXPERIMENT

A. The experimental cell

Particle adsorption experiments were performed using the direct microscope observation method in the cell shown schematically in Fig. 1(a), referred to later on as the diffusion cell (DC). The main part of the cell was a Teflon container of internal dimension $1.5\times2.5\times8$ cm with a rectangular window in which a mica sheet was inserted, used as the substrate for particle adsorption. The container was placed under the microscope fixed to a movable stage which could be inclined (rotated) by an angle φ varied between zero (the microscope oriented perpendicular as usual) and 90° with the microscope oriented horizontally. In the latter case, gravity was directed parallel to the mica sheet. With this arrangement, particle adsorption kinetics and distribution over mica surface could be followed *in situ* using a video camera (Hamamatsu type C-3077) coupled with an image processor and video recorder.

Except for the diffusion cell, some reference experiments were carried out in the impinging-jet cell shown schematically in Fig. 1(b). The cell, used extensively before for similar studies,[5,6,10,11] consisted of a capillary tube of circular cross section (internal diameter 0.2 cm) through which the particle suspension was driven due to hydrostatic pressure difference. The pressure gradient determined the volumetric flow rate Q of the suspension which was kept constant during an experiment. The suspension stream leaving the capillary was directed towards a perpendicularly placed mica sheet held fixed to the external tubing B due to the underpressure prevailing in the cell. The suspension leaving the external tube was discarded. In this cell, the direction of gravity was perpendicular and opposite to the mica/liquid interface.

B. Materials and methods

The colloid particles used in our adsorption studies were polystyrene latex suspensions synthesized in a surfactant-free polymerization reaction carried out according to the method described in Ref. 12. The latex suspension were charge stabilized by ionic groups stemming from the initiator. By using a persulfate initiator, negatively charged suspensions were synthesized whereas the use of the 2,2′-azobis (2-amidinopropane) dihydrochloride (ABA) initiator lead to positively charged lattice suspensions. After synthesis, the latex was purified by steam distillation and by prolonged membrane filtration until the conductivity of filtrate reached the value of water used for washing. The filtrates were also checked for the presence of traces of initiator and nonreacted styrene using UV spectroscopy. The size distribution of latex suspensions was determined by ZM Coulter Counter. The latex was stored in the form of a concentrated stock suspension (10% by weight) which was indefinitely stable. Prior to each experiment the suspension was diluted to the desired number concentration, whose value was determined by Coulter Counter.

Zeta potential of latex particles was determined as a function of ionic strength by microelectrophoresis using the Brookhaven Zeta Pals apparatus. The crystallized KCl was used for preparing the electrolyte solutions in triply distilled water. The pH of these suspensions was equal to 5.8.

In our studies three latex samples were used: L18, L70 (both negatively charged), and L+39 (positively charged). For the sake of convenience the basic characteristics of these lattices have been collected in Table I.

Natural ruby mica sheets, supplied by Mica and Micanite Supplies Ltd., England, were used as substrates in the adsorption experiments. In the case of positive latex, freshly cleaved mica sheets were used without any pretreatment, whereas for negative latex, mica sheets were conditioned in 2×10^{-4} M $AlCl_3$ solution for 24 h at 80 °C. This procedure converted the natural negative charge of mica to positive charge which assured irreversible adsorption of negatively charged latex particles. Before each experiment sheets were thoroughly rinsed with distilled water and put on the top of the cell without letting the liquid film to evaporate.

Zeta potential of mica sheets was determined using the

TABLE I. Colloid particle characteristics.

Colloid system	Size [μm]	Density at 20 °C	Zeta potential[a] ζ[mV]
Latex L18	1.0 ± 0.08	1.05	−54
Latex L70	0.87 ± 0.07	1.05	−50
Latex L+39	1.1 ± 0.08	1.05	+50

[a]At $I=10^{-4}$ M.

streaming potential method in the plane-parallel cell described in detail elsewhere.[13] Two thin mica sheets were placed between the Teflon blocks separated by a 0.025 cm thick Teflon gasket serving as a spacer. The parallel plate channel was formed by clamping the Teflon blocks together with two mica sheets and the spacer between them, using a press under constant torque conditions.

The streaming potential E_s, occurring when an electrolyte was flowing through the cell under regulated and constant hydrostatic pressure difference, was measured using the two Ag/AgCl electrodes. The zeta potential of the mica sheets was calculated using the improved Smoluchowski formula, accounting for the contribution stemming from spacer walls.[13] It was found that the zeta potential of bare (untreated) mica was varied between -60 ± 5 mV and -90 ± 8 mV, for the ionic strength 10^{-3} M and 2×10^{-5} M KCl used in our experiments. On the other hand, the $AlCl_3$ treated mica exhibited the zeta potential of $+30$ to $+60$ mV for the same range of ionic strength.

Particle adsorption experiments involving the DC have been carried out according to a carefully elaborated procedure aimed at minimizing the nonuniform concentration distribution effects. Hence, the cell with the freshly mounted mica window was fastened on the microscope stage and the whole set was inclined to the horizontal position. Then, the cell was filled with a stirred latex suspension of appropriate particle concentration and particle adsorption was followed *in situ* in real time using the video recorder system. The recorded signal was used subsequently for evaluating the kinetic adsorption curves, i.e., the dependencies of surface concentration on adsorption time *t*. The surface concentration of adsorbed particles *N* was obtained by counting the number of particles N_p found over a given surface area ΔS, typically the size of a few thousands μm^2. The dimensionless surface coverage was then calculated as $\Theta=\pi a^2\langle N_p\rangle/\Delta S$ (where *a* is the particle radius and $\langle N_p\rangle$ is the averaged value of N_p).

The variance of particle distributions was determined according to a different procedure. First, particle adsorption was continued until the desired surface coverage Θ was attained (this adsorption time was estimated from previously recorded kinetic curves). Then, the adsorption experiment was stopped by replacing the latex suspension by pure electrolyte solution and images of irreversible adsorbed particles were collected over equal-sized, nonoverlapping larger surface areas ΔS chosen at random over the interface. The areas ΔS were divided into subareas Δs in such a way that the averaged surface concentration $\langle N_p/\Delta s\rangle$ was equal to approximately 40 or 10. The number of the areas was varied between 100 and 500 in order to make the overall number of particles counted equal 5000–20 000. It should also be pointed out that due to very large observation area of the DC cell, comparable with cm^2 the overall population of adsorbed particles was very large, exceeding 10^6 for $\Theta>0.02$. This ensured that the explicit and implicit size effects connected with a finite number of particles within the population used for variance analysis could be entirely neglected. The relative variance of particle concentration distribution was calculated directly from the definition

$$\overline{\sigma^2}=\frac{\Sigma_{n=1}^{n_a}[\langle N_p\rangle-N_p]^2}{\langle N_p\rangle}=\frac{\langle N_p^2\rangle-\langle N_p\rangle^2}{\langle N_p\rangle},$$

where n_a is the number of subareas Δs.

A very similar procedure was used for determining the variance in the case of the impinging-jet cell. Particle suspension was driven through the cell at such a rate *Q* that the Reynolds number $\mathrm{Re}=Q/\pi R\nu$ (where ν is the liquid kinematic viscosity) was very low, equal to 0.6. Then, after the desired adsorption time calculated from previous kinetic experiments, pure electrolyte solution was streamed through the cell and the variance of adsorbed particle distribution was determined as above.

Since many experiments on particle adsorption kinetics have been done in the literature in a stepwise manner,[7–9] we have also performed a series of variance measurements in this way. In this case, freshly cleaved mica sheet was immersed in a latex particle suspension. After a given adsorption time (ranging from 15 min to 80 h) the samples were removed from the suspension and carefully rinsed with triply distilled water without allowing the water film to evaporate. Then, the wet sheet in contact with electrolyte for the whole time was placed under the microscope. Images taken from various areas, chosen at random, were used for evaluating the averaged surface concentration of particles and the variance as described above.

III. RESULTS AND DISCUSSION

All experiments reported hereafter were performed at *p*H 5.8 for three ionic strength values equal to 10^{-3}, 10^{-4}, and 2×10^{-5} M, fixed by addition of a given amount of KCl. For this range of ionic strength the latex suspensions were indefinitely stable, showing no presence of aggregates in the bulk as checked in a series of preliminary experiments. Similarly, aggregates have very infrequently been found at the surface so their presence can be neglected. This can qualitatively be observed in the micrographs shown in Fig. 2 obtained for the L18 latex for $I=10^{-4}$ M and $n_b=5.16\times10^9\ cm^{-3}$ ($\Theta=0.1$ and 0.3, respectively). As can be observed in this figure, particle distributions are statistically uniform with no tendency to clustering, as is often the case when the particle monolayer is dried before microscope examination. This confirms that the particles once adsorbed were irreversibly bound to the surface with no tendency to lateral motion.

The uniformity of particle distribution was confirmed quantitatively by a thorough variance analysis of particle surface concentration performed according to the method described above. The grid used for variance determination ($\langle N_p\rangle=10$) is also shown in Fig. 2. In order to select proper surface concentration range for variance analysis, a series of kinetic experiments has been performed in which the dependence of Θ on adsorption time was determined for various ionic strength. These experiments have been discussed in some detail elsewhere.[9] Here, we present typical results obtained for the L18 latex for the above ionic strength values. As can be seen in Fig. 3, the increase in Θ can be expressed

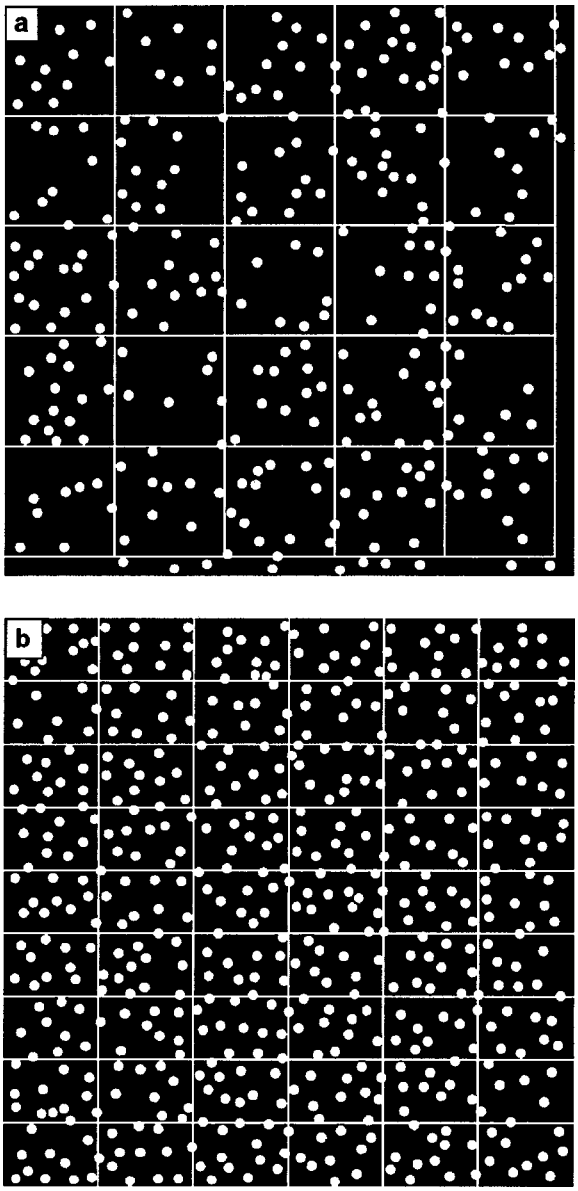

FIG. 2. The micrographs showing the distribution of adsorbed latex particles at mica obtained for $I=10^{-4}$ M. (a) $\Theta=0.1$, (b) $\Theta=0.3$.

for short times as a linear function of the square root of time, i.e.,

$$\Theta=\pi a^2 2n_b\sqrt{D_\infty t}, \tag{1}$$

where D_∞ is the diffusion coefficient of a particle calculated from the Stokes equation, equal to 4.3×10^{-9} cm^2/s for the L18 latex. Validity of this equation indicates that in our experiments particle adsorption occurred under purely diffusional transport mechanism with no contribution due to natural convection, as observed by Semmler *et al.*[8]

However, for adsorption time longer than 1 h, when Θ exceeded 0.2, the experimental data deviate significantly from the square root of time dependence as a result of surface exclusion effects (often called blocking effects) discussed extensively elsewhere.[11] The experimental kinetic runs were interpreted in terms of the theoretical approach based on numerical solution of the bulk mass transfer equation with the nonlinear boundary condition, describing the

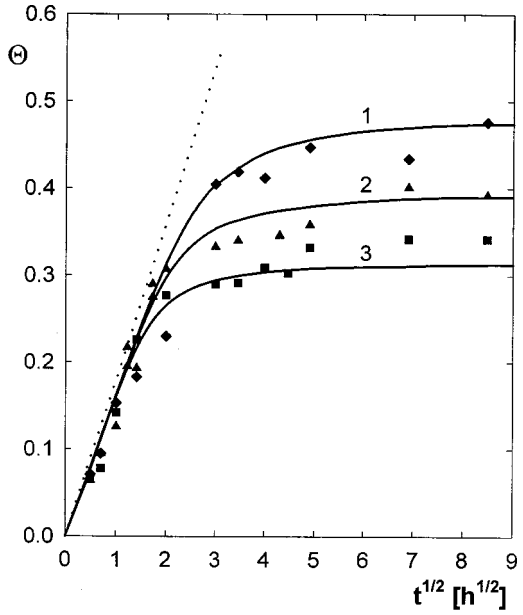

FIG. 3. Adsorption kinetics of latex particles (the L18 sample) at mica expressed as the coverage Θ vs $\sqrt{t}$ dependencies; $n_b=5.16\times10^9$ cm^{-3}. (1) ◆ for $I=10^{-3}$ M; (2) ▲ for $I=10^{-4}$ M; (3) ■ for $I=2\times10^{-5}$ M. The continuous lines denote the exact numerical solutions of the diffusion transport equation with the blocking function calculated from Eq. (2); the dotted line shows the results stemming from the limiting formula $\Theta=\pi a^2 2n_b\sqrt{D_\infty t}$.

surface exclusion effects.[9] The blocking function $B(\Theta)$ used for expressing the boundary conditions was taken from the classical RSA model. It was approximated by the equation[9]

$$B(\Theta)=(1+0.812\overline{\Theta}+0.426\overline{\Theta}^2+0.0716\overline{\Theta}^3)(1-\overline{\Theta})^3, \tag{2}$$

where $\overline{\Theta}=\Theta/\Theta_{mx}$ and Θ_{mx} is the maximum (saturation) coverage. As can be observed in Fig. 3, the theoretical results, marked by the solid lines, describe well the experimental data for the entire range of adsorption time. A characteristic feature of the kinetic runs shown in Fig. 3 is that for very long adsorption time a limiting (saturation) value of Θ is attained (Θ_{mx}) which increases with ionic strength of the suspension. It was determined experimentally that for adsorption time of 80 h the limiting Θ_{mx} values were 0.47, 0.40, and 0.34 for $I=10^{-3}$, 10^{-4}, and 2×10^{-5} M, respectively. For the sake of convenience these data are collected in Table II. Notice that the value of 0.47 determined for $I=10^{-3}$ M approaches close to the limiting value for hard (noninteracting) spheres, found by numerical simulation to be 0.547. It is interesting that this limiting (jamming) value is the same for the random sequential adsorption (RSA) and

TABLE II. Latex L18 data.

$I[M]$	$(\kappa a)^{-1}$	h^*/a	Θ_{mx} (theoretical)	Θ_{mx} (experimental)
10^{-3}	0.019	0.05[a]	0.49[a]	0.47
10^{-4}	0.060	0.17[a]	0.40[a]	0.40
2×10^{-5}	0.135	0.36[b]	0.32[b]	0.34

[a]Values calculated from Eqs. (3) and (4).
[b]Values obtained from Monte Carlo simulations.

diffusion random sequential adsorption (DRSA) models.[14] By contrast, in the case of the ballistic model the limiting Θ_∞ value was found to be 0.62.[15]

The deviation of the value measured for $I=10^{-3}$ M from the hard particle jamming limit can be attributed to the electrostatic repulsion between the adsorbed and adsorbing particles. The range of these interactions is governed primarily by the double-layer thickness given by the expression

$$Le/a=(\kappa a)^{-1}=(\varepsilon kT/8\pi e^2 I a^2)^{1/2},$$

where ε is the dielectric constant of water, k is the Boltzmann constant, T is absolute temperature, and e is the elementary charge.

The values of the Le/a parameter calculated for the L18 latex at various ionic strength are listed in Table II.

Knowing Le, one can calculate the effective range of electrostatic interaction h^* from the formula derived elsewhere[16]

$$\frac{h^*}{a}=\frac{1}{2}(\kappa a)^{-1}\left[\ln\frac{u_0}{u_{ch}}-(\kappa a)^{-1}\ln\left(1+\frac{h_0^*}{a}\right)\right], \tag{3}$$

where $h_0^*/a=1/2(\kappa a)^{-1}\ln(u_0/u_{ch})$, $u_0=8\varepsilon a(kT/e)^2\times\tanh^2(\zeta e/4kT)$, ζ is the zeta potential of the particle, and u_{ch} is the characteristic energy equal to 1.5 kT.[9]

As can be seen in Table II, the h^*/a parameter varies between 5% of particle geometrical radius for $I=10^{-3}$ M to 36% for $I=2\times10^{-5}$. Using the h^* concept, one can also estimate the maximum coverage for interacting particles from the formula[9]

$$\Theta_{mx}=\Theta_\infty\frac{1}{\left(1+\frac{h^*}{a}\right)^2}. \tag{4}$$

As can be deduced from Table II, the theoretical predictions stemming from Eq. (4) agree reasonably well with our experimental data. This behavior was observed for other experimental systems as well,[7,8,11] which suggests that the effective hard particle concept is useful for interpretation of adsorption kinetic measurements involving electrostatically interacting particles.

One of the goals of this work was to check if the effective hard particle concept is also applicable for interpretation of experimental results concerning density fluctuations in adsorbed particle layers. In Fig. 4 the dependence of $\overline{\sigma^2}$ on particle coverage Θ is presented, obtained for the highest ionic strength $I=10^{-3}$ M when the correction due to electrostatic repulsion remains rather minor. As can be seen, the data obtained for $\langle N_p\rangle=10$ are for the entire Θ range studied (0.03–0.45), well above analogous data determined for $\langle N_p\rangle=40$. This deviation seems to confirm the theoretical predictions elaborated in Refs. 17 and 18 suggesting that due to boundary effects the $\overline{\sigma^2}$ vs Θ dependence for finite-sized systems should be given be the equation

$$\overline{\sigma^2}=\overline{\sigma_0^2}+\left(\frac{\pi a^2}{\Delta s}\right)^{1/2}y_1(\Theta)+\frac{\pi a^2}{\Delta s}y_2(\Theta), \tag{5}$$

where $\overline{\sigma_0^2}$ is the reduced variance for an infinite subsystem, Δs is the area of the subsystem, and $y_1(\Theta)$, $y_2(\Theta)$ are the correction functions. Roman *et al.*[18] have determined these functions analytically up to the order of Θ^2 for the RSA case, whereas Senger *et al.*[17] gave numerical fits valid for an arbitrary range of Θ in the form

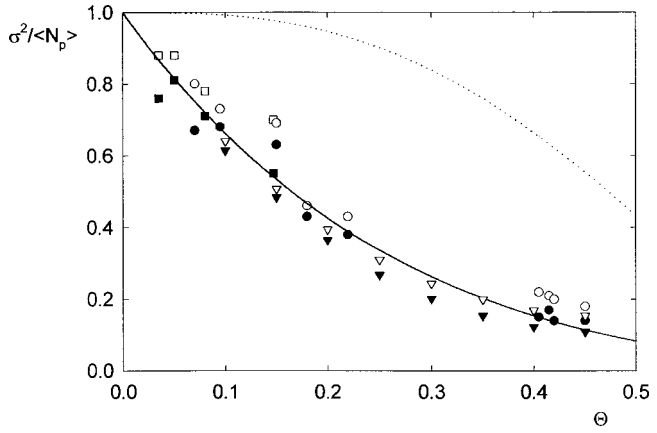

FIG. 4. The $\sigma^2/\langle N_p\rangle$ dependence on the coverage Θ; the points denote experimental results obtained for ionic strength $I=10^{-3}$ M. ■ for the L+39 latex, $\langle N_p\rangle=40$; □ for the L+39 latex, $\langle N_p\rangle=10$; ● for the L18 latex, $\langle N_p\rangle=40$; ○ for the L18 latex, $\langle N_p\rangle=10$. The inverted triangles denote the RSA simulation results (full symbols for $\langle N_p\rangle=40$ and empty symbols for $\langle N_p\rangle=10$); the continuous line denotes the results stemming from the SPT theory, Eq. (7), and the dotted line represents the theoretical predictions derived from the ballistic model.

$$\begin{aligned} y_1&=\frac{64}{3\pi^{3/2}}\Theta-7.14\Theta^2-2.22\Theta^3+9.76\Theta^4,\\ y_2&=-0.778\Theta+3.72\Theta^2-8.48\Theta^3+6.07\Theta^4. \end{aligned} \tag{6}$$

In our case, for $\langle N_p\rangle=40$ and $\Theta=0.05$, the surface area of the subsystem $\Delta s=\langle N_p\rangle\pi a^2/\Theta$ was $630\,\mu\text{m}^2(6.3\times10^{-6}\,\text{cm}^2)$; thus, the ratio $\pi a^2/\Delta s$ was equal to 0.0011. This indicates that the correction due to the y_2 function was negligible, whereas the correction stemming from the y_1 function was 0.006, which is less than 1% of the measured $\overline{\sigma^2}$ value. For $\langle N_p\rangle=10$, the correction to the measured $\overline{\sigma^2}$ is about 1.5%. As can be seen in Fig. 4, the difference among the experimental data measured for $\langle N_p\rangle=40$ and $\langle N_p\rangle=10$ was considerably larger than this estimate, about 5%–10%. One may suspect, therefore, that beside the systematic deviation connected with the boundary effects another source of experimental scatter appeared. This was probably due to uncertainty in assigning particles located to the boundary to a given surface element. This effect is expected to increase proportionally with the ratio of the number of particles close to the periphery to the overall number of particles on the area, i.e., to the $(a^2/\Delta s)^{1/2}$, analogously as for the y_2 function.

For $\Theta=0.4$, according to Eq. (6), the correction stemming from the y_2 function equals 0.047 for $\langle N_p\rangle=40$ and 0.095 for $\langle N_p\rangle=10$. As can be seen in Fig. 4, unlike the low coverage limit, this theoretical prediction is in good agreement with experimentally observed difference in $\overline{\sigma^2}$ between $\langle N_p\rangle=40$ and $\langle N_p\rangle=10$. From this estimation one may expect that for higher surface coverage, $\overline{\sigma^2}$ measured for subsystems of very large surface area (when $\langle N_p\rangle\to\infty$) should be about 0.05 smaller than the experimental data shown in

Fig. 4 for $\langle N_p \rangle = 40$. However, a direct experimental proof of this predictions would be difficult due to the necessity of considering very large particle populations and limited quality of the image for high coverage as a result of multiple light scattering.

These analytical estimates, derived for the RSA model, are further supported by the good agreement of the experimental data with the numerical simulations, also shown in Fig. 4 by reversed triangles. The simulations were performed according to the RSA model of soft (interacting) spheres as described in detail elsewhere.[6,11,16] This finding is rather unexpected because in the RSA model all effects associated with particle diffusion are neglected. One may therefore suspect that the agreement is due to the limited accuracy of the experimental method and cannot be exploited as a decisive proof to validate the RSA model. Indeed, the results derived for equilibrium systems from the scaled particle theory[19,20] (SPT) also reflect well the experimental data for the entire range of coverage. In this case, $\overline{\sigma}^2$ is given by the analytical formula

$$\overline{\sigma}^2 = \pi a^2 kT \left(\frac{\partial p}{\partial \Theta} \right)^{-1} = \frac{(1-\Theta)^3}{1+\Theta}, \tag{7}$$

where p is the *2D* pressure of the equilibrium hard sphere fluid.

The good agreement between experimental data and the SPT theory is probably due to compensation of the above analyzed boundary effect with the error associated with particle interactions described by the h^*/a parameter. Both effects, acting oppositely, are of the order of 0.05 (in absolute numbers) for the range of surface coverage 0.3–0.5.

Despite these limitations, however, the results shown in Fig. 4 demonstrate quite unequivocally that the dependence of $\overline{\sigma}^2$ on Θ measured for diffusion controlled transport conditions deviates in character from that predicted by the ballistic model[1–3] depicted in Fig. 4 by the dotted line. In this respect our results differ from previous measurements discussed in Refs. 1–4. This can be attributed to the gravity effects which were always present in those experiments.

The data discussed above were obtained under conditions when the electrostatic interactions played a minor role so their influence on $\overline{\sigma}^2$ was of the order of experimental error. For lower ionic strength, due to increased value of h^*/a as discussed above, the role of electrostatic interactions should be more significant. This can be observed in Figs. 5 and 6, where the data obtained for $I = 10^{-4}$ and $I = 2 \times 10^{-5}$ M are collected. In Fig. 5 we have also shown for comparison the results obtained in the impinging-jet cell at Re=0.6. Despite the spread of experimental data, one can deduce that there was no statistically significant difference among results obtained for different cells and lattices (either positively or negatively charged). Analogously, as for $I = 10^{-3}$ M, in the case of lower ionic strength the results obtained for $\langle N_p \rangle = 40$ are well below the results determined for $\langle N_p \rangle = 10$. It also seems that the simulations performed according to the RSA model are in good agreement with the experimental data for lower ionic strength as well. In contrast, the analytical results calculated from Eq. (7) for an equilibrium hard particle system overestimate the experimental data, especially for the lowest ionic strength value. Since this deviation is well above the experimental error bound, one may conclude that the results shown in Figs. 5 and 6 confirm unequivocally the significance of electrostatic interactions in fluctuation phenomena within adsorbed particle layers. A quantitative interpretation of this behavior was attempted by introducing the above effective hard particle concept. Within the scope of this model, the effective particle coverage $\overline{\Theta}$ is defined in analogy to Eq. (4) as follows:

$$\overline{\Theta} = \Theta (1 + h^*/a)^2. \tag{8}$$

Using this definition, all the experimental results obtained for various ionic strength can be transformed to one universal dependence $\overline{\sigma}^2$ vs $\overline{\Theta}$, which is plotted in Fig. 7. As can be

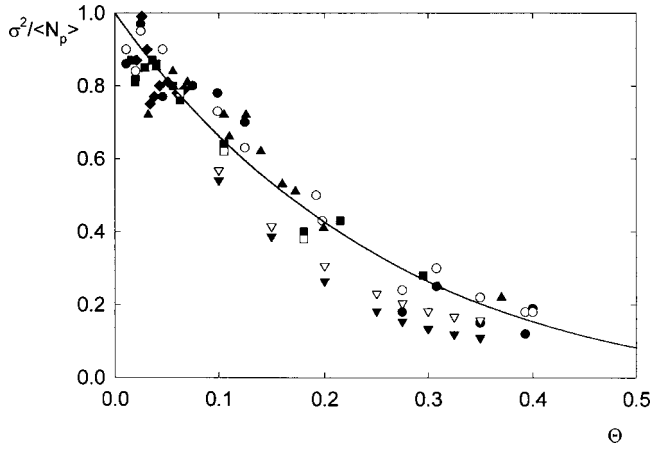

FIG. 5. The $\sigma^2/\langle N_p \rangle$ vs the coverage Θ; the points denote experimental results obtained for ionic strength $I = 10^{-4}$ M. ■ for the L+39 latex, $\langle N_p \rangle = 40$; ◆ for the L+39 latex in the impinging-jet cell, $\langle N_p \rangle = 40$; □ for the L+39 latex, $\langle N_p \rangle = 10$; ● for the L18 latex, $\langle N_p \rangle = 40$; ○ for the L18 latex, $\langle N_p \rangle = 10$, ▲ for the L70 latex, $\langle N_p \rangle = 40$. The inverted triangles denote the RSA simulation results (full symbols for $\langle N_p \rangle = 40$ and empty symbols for $\langle N_p \rangle = 10$); the continuous line denotes the results stemming from the SPT theory, Eq. (7).

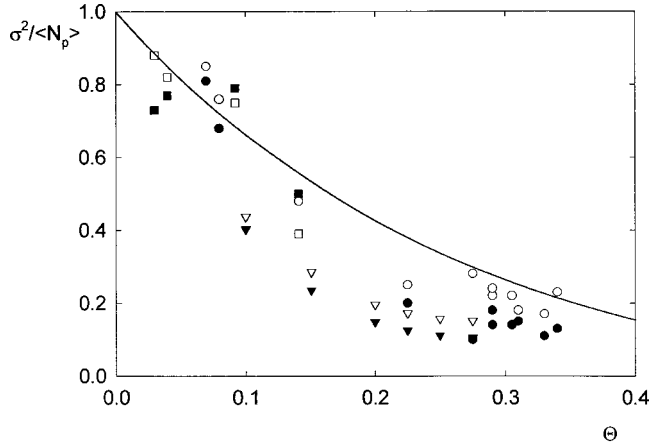

FIG. 6. The $\sigma^2/\langle N_p \rangle$ dependence on the coverage Θ; the points denote experimental results obtained for ionic strength $I = 2 \times 10^{-5}$ M. ■ for the L+39 latex, $\langle N_p \rangle = 40$; □ for the L+39 latex, $\langle N_p \rangle = 10$; ● for the L18 latex, $\langle N_p \rangle = 40$; ○ for the L18 latex, $\langle N_p \rangle = 10$. The inverted triangles denote the RSA simulation results (full symbols for $\langle N_p \rangle = 40$ and empty symbols $\langle N_p \rangle = 10$); the continuous line denotes the results stemming from the SPT theory, Eq. (7).

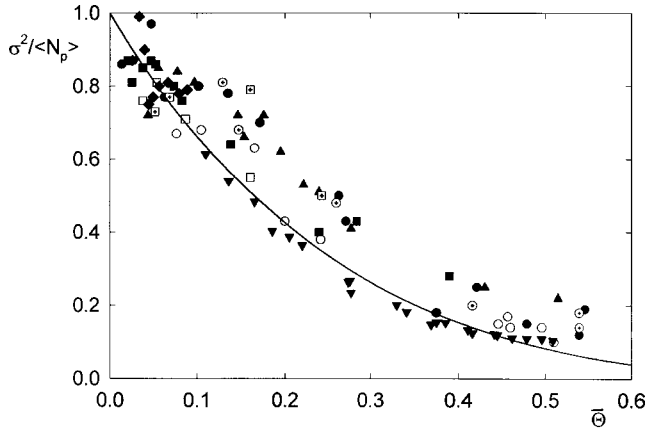

FIG. 7. The universal graph showing the dependence of $\sigma^2/\langle N_p\rangle$ on the effective coverage $\bar{\Theta}=\Theta(1+h^*/a)^2$; the points denote the transformed experimental results obtained for $\langle N_p\rangle=40$. □ for the L+39 latex, I $=10^{-3}$ M; ■ for the L+39 latex, I$=10^{-4}$ M; ♦ for the L+39 latex in the impinging-jet cell, I$=10^{-4}$ M; ⊞ for the L+39 latex, I$=2\times10^{-5}$ M; ○ for the L18 latex, $I=10^{-3}$ M; ● for the L18 latex, $I=10^{-4}$ M; ⊕ for the L18 latex, $I=2\times10^{-5}$ M; ▲ for the L70 latex $I=10^{-4}$ M. The inverted triangles (full symbols) denote the RSA simulation results and the continuous line denotes the results stemming from the SPT theory, Eq. (7).

seen, the experimental data corrected in this way can be well accounted for by the theoretical dependence stemming from Eq. (7), valid for hard particle equilibrium systems. However, a statistically significant deviation from the ''master curve'' is observed for the moderate surface coverage range, i.e., $0.1<\bar{\Theta}<0.3$ and lower ionic strength, which suggests that the effective hard particle concept can only be treated as an approximate model. Nevertheless, the data shown in Fig. 7, covering practically the entire range of ionic strength occurring in experiments carried out under diffusion controlled transport conditions, can be exploited as useful reference values for estimating accuracy of variance measurements.

IV. CONCLUDING REMARKS

The direct observation method applied in this work proved useful for a quantitative determination of fluctuation phenomena occurring under diffusion controlled adsorption regime pertinent to colloids and proteins. The experimental results demonstrated that for higher ionic strength the dependence of $\bar{\sigma}^2$ on adsorbed particle density can satisfactorily be described by the RSA model and the SPT theory, formulated for 2D equilibrium phase of hard spheres. Our finding differs, therefore, from the ballistic model predictions.

The results obtained for lower ionic strength, when electrostatic interactions among particles become significant, can be accounted for in an approximate way by introducing the effective hard particle concept.

It can be expected that the universal graph showing the $\sigma^2/\langle N_p\rangle$ vs $\bar{\Theta}$ dependence can be exploited for detecting any heterogeneities in surface charge or initial particle concentration distribution.

The results obtained support the hypothesis that colloid particles susceptible for direct *in situ* observations can be used as convenient systems to mimic fluctuations occurring in equilibrium systems.

ACKNOWLEDGMENT

This work was partially supported by the KBN Grant No. 3 T09A 105 18.

[1] P. Wojtaszczyk, E. K. Mann, B. Senger, J. C. Voegel, and P. Schaaf, J. Chem. Phys. **103**, 8285 (1995).
[2] P. Schaaf, P. Wojtaszczyk, B. Senger, J. C. Voegel, and H. Reiss, Phys. Rev. E **51**, 4292 (1995).
[3] P. Schaaf, P. Wojtaszczyk, E. K. Mann, B. Senger, J. C. Voegel, and D. Bedeaux, J. Chem. Phys. **102**, 5077 (1995).
[4] E. K. Mann, P. Wojtaszczyk, B. Senger, J. C. Voegel, and P. Schaaf, Europhys. Lett. **30**, 261 (1995).
[5] Z. Adamczyk and L. Szyk, Bull. Pol. Acad. Sci., Chem. **43**, 244 (1995).
[6] Z. Adamczyk, B. Siwek, L. Szyk, and M. Zembala, J. Chem. Phys. **105**, 5552 (1996).
[7] C. A. Johnson and A. M. Lenhoff, J. Colloid Interface Sci. **179**, 587 (1996).
[8] M. Semmler, E. K. Mann, J. Ricka, and M. Borkovec, Langmuir **15**, 5127 (1998).
[9] Z. Adamczyk and L. Szyk, Langmuir **16**, 5730 (2000).
[10] Z. Adamczyk, M. Zembala, B. Siwek, and P. Warszyński, J. Colloid Interface Sci. **140**, 123 (1990).
[11] Z. Adamczyk, B. Siwek, M. Zembala, and P. Belouschek, Adv. Colloid Interface Sci. **48**, 151 (1994).
[12] J. W. Goodwin, J. Hearn, C. C. Ho, and R. Ottewill, Colloid Polym. Sci. **252**, 464 (1974).
[13] M. Zembala and Z. Adamczyk, Langmuir **16**, 1593 (2000).
[14] B. Senger, P. Schaaf, J. C. Voegel, A. Johner, A. Schmitt, and J. Talbot, J. Chem. Phys. **97**, 3813 (1992).
[15] R. Jullian and P. Meakin, J. Phys. A **25**, 489 (1992).
[16] Z. Adamczyk, B. Siwek, and M. Zembala, J. Colloid Interface Sci. **151**, 351 (1992).
[17] B. Senger, P. Schaaf, J. C. Voegel, P. Wojtaszczyk, H. Reiss, Proc. Natl. Acad. Sci. U.S.A. **191**, 10029 (1994).
[18] F. L. Roman, J. A. White, and S. Velasco, J. Chem. Phys. **106**, 4196 (1997).
[19] T. Boublik, Mol. Phys. **29**, 421 (1975).
[20] Z. Adamczyk and P. Weroński, J. Chem. Phys. **107**, 3691 (1997).